How to cite: *Angew. Chem. Int. Ed.* **2022,** *61,* e202201847
International Edition: doi.org/10.1002/anie.202201847
German Edition: doi.org/10.1002/ange.202201847

Solar Cells Hot Paper

Pyrene-Based Dopant-Free Hole-Transport Polymers with Fluorine-Induced Favorable Molecular Stacking Enable Efficient Perovskite Solar Cells

Zhaoyang Yao[+], Fuguo Zhang[+], Lanlan He, Xingqi Bi, Yaxiao Guo, Yu Guo, Linqin Wang, Xiangjian Wan, Yongsheng Chen, and Licheng Sun**

Abstract: A new class of polymeric hole-transport materials (HTMs) are explored by inserting a two-dimensionally conjugated fluoro-substituted pyrene into thiophene and selenophene polymeric chains. The broad conjugated plane of pyrene and "Lewis soft" selenium atoms not only enhance the π–π stacking of HTM molecules greatly but also render a strong interaction with the perovskite surface, leading to an efficient charge transport/transfer in both the HTM layer and the perovskite/HTM interface. Note that fluorine substitution adjacent to pyrene boosts the stacking of HTMs towards a more favorable face-on orientation, further facilitating the efficient charge transport. As a result, perovskite solar cells (PSCs) employing **PE10** as dopant-free HTM afford an excellent efficiency of 22.3 % and the dramatically enhanced device longevity, qualifying it among the best PSCs based on dopant-free HTMs.

Introduction

Perovskite solar cells (PSCs) have afforded a certified power conversion efficiency (PCE) of 25.7 % thus far, mainly benefiting from the unrivalled photoelectric characteristics of organic–inorganic hybrid perovskite crystals.[1] In a classic PSC with n-i-p structure, a hole-transport material (HTM) is an irreplaceable component for efficient hole extraction, reverse electron flow blocking and protection of moisture-sensitive perovskites. Now almost all the state-of-the-art PSCs were achieved by using doped 2,2′,7,7′-tetrakis(*N*,*N*-di-*p*-methoxyphenylamine)-9,9′-spirobifluorene (spiro-OMeTAD) as the HTM. However, due to the huge steric hindrance of spiro structure, several delicately selected dopants are indispensable to address the large film resistivity of spiro-OMeTAD.[2] Unfortunately, the widely applied dopants, e.g. lithium salts, pyridine analogs and metal complexes, are either hygroscopic or volatile,[3] and even can migrate in the HTM layer to some extent due to their noncovalent bond properties.[4] This could result in severe morphology deterioration of both perovskite crystals and HTM layers, making the doping strategy impracticable for large-scale production of PSCs. That is why the innovative exploration for dopant-free HTMs featuring both economic feasibility and high efficiency has attracted urgent attention.[5] However, very few first-class dopant-free HTMs have been established so far due to their harsh and multiple prerequisites for energy levels, charge transport, interfacial contact and passivation, etc.

Conjugated polymers have been regarded as a promising candidate for commercially feasible dopant-free HTMs[6] due to their excellent carrier mobility, film-forming capacity, thermal and optical stabilities. Although polymers as dopant-free HTMs have been applied in PSCs with relatively high efficiencies,[7] nearly all of them are characteristic of sophisticated structures with alternately appearing ring-fused donors (D) and heterocyclic acceptors (A), rendering them unaffordable for industrial production in the

[*] Z. Yao,[+] X. Bi, X. Wan, Y. Chen
Key Laboratory of Functional Polymer Materials,
College of Chemistry, Nankai University
Tianjin 300071 (China)
E-mail: yschen99@nankai.edu.cn

Z. Yao,[+] F. Zhang,[+] Y. Guo, L. Sun
Department of Chemistry, Organic Chemistry,
KTH Royal Institute of Technology
Stockholm 10044 (Sweden)
E-mail: lichengs@kth.se

L. He
Department of Chemistry, Applied Physical Chemistry,
KTH Royal Institute of Technology
Stockholm 10044 (Sweden)

Y. Guo
State Key Laboratory of Separation Membranes and Membrane Processes, School of Chemistry, Tiangong University,
Tianjin 300387 (China)

Y. Guo, L. Wang, L. Sun
Center of Artificial Photosynthesis for Solar Fuels,
School of Science, Westlake University,
Hangzhou 310024 (China)

[+] These authors contributed equally to this work.

near future. To address this issue, our group has developed a series of cost-effective polymeric HTMs without strong D–A features by replacing structurally complicated heterocyclic acceptors with simple thiophene analogs.[8] More importantly, a semi-empirical guideline was put forward for material design indicating that a successful dopant-free polymeric HTM should include several key structural elements of two dimensionally (2D) conjugated polycyclic aromatic hydrocarbons (PAHs), "Lewis soft" heteroatoms, bulky hydrophobic aliphatic chains and so on.[8b,c] Bearing this in mind, excellent PSCs based on polymeric HTMs have been afforded with approaching 22 % PCEs. Nevertheless, it is believed that the best performance of PSCs, including PCE, stability and even cost, are far from achieved by polymeric HTMs, especially in view of the champion PCE of 25.7 % already afforded by PSCs based on spiro-OMeTAD.

Based on our reported semi-empirical guideline for molecular design,[8b] sufficient bulky hydrophobic aliphatic chains are essential in polymeric HTMs if excellent device stability is to be achieved. Whereas aliphatic chains usually inhibit the tight stacking of polymer strands and also the strong interaction with perovskite surface, thus leading to the inefficient charge transport in HTM layers and suppressed charge transfer at HTM/perovskite interface. That is why large 2D conjugated PAHs, which could mitigate the sharp contradiction between hydrophobicity and charge transport/transfer, are usually indispensable in polymeric HTMs with high performance. Note that the selection of 2D PAH is very crucial in HTM design, which should possess a broad conjugated plane for strong molecular packing, adequate chemical active sites for both energy level and configurational tuning, suitable dihedral angles when connecting with bridged thiophene units, etc. Therefore, there are not so many PAH candidates qualifying for the ideal building block of polymeric HTMs. Among the numerous PAHs, pyrene as a multifunctional building block[9] is expected to well meet the requirements above, despite that, it is rarely employed in polymeric HTMs now. With this in mind, pyrene has been incorporated into thiophene and selenophene polymeric chains to synthesize a series of dopant-free HTMs (Figure 1, **PE7**–**PE10**) in this work. The broad conjugated plane of pyrene is expected to pack tightly with not only adjacent polymer strands but also the perovskite surface. In addition, the four chemically active sites on pyrene make the structural modification quite ease in molecular design of HTMs.[9a] Taking this advantage, various fluorine atoms were introduced on the pyrene to fine-tune the energy levels and configurations of HTMs. In addition, due to the easy polarizable feature and larger atomic radius of selenium (≈103 pm) than that of sulfur (88 pm), the selenium has been verified as the more effective passivator to stabilize the uncoordinated lead sites at HTM/perovskite interface for the first time in our previous work.[8b] As a result, with the aid of favorable face-on molecular stacking induced by fluorine-aromatic (F–π) interaction[10] and adequate interfacial passivation caused by Pb–Se noncovalent bond,[8b] dopant-free **PE10** based PSC affords an excellent PCE of 22.3 %, ranking it among the best PSCs based on dopant-free HTMs.

Results and Discussion

Scheme 1 and S1–S4 illustrated the synthetic routes to **PE7**–**PE10** polymers and their corresponding model molecules. The characterizations of intermediates and targeted molecules were listed in Figure S19–S126 and the detailed procedures were described in Supporting Information. Note that all the polymers can be easily synthesized with over 85 % yield in each step from commercially available raw

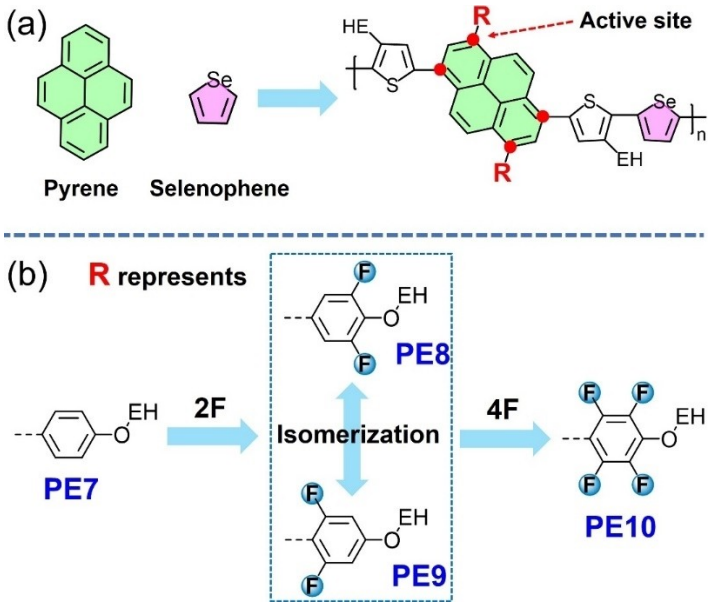

Figure 1. Four **PE** polymers with various fluorine substitutions.

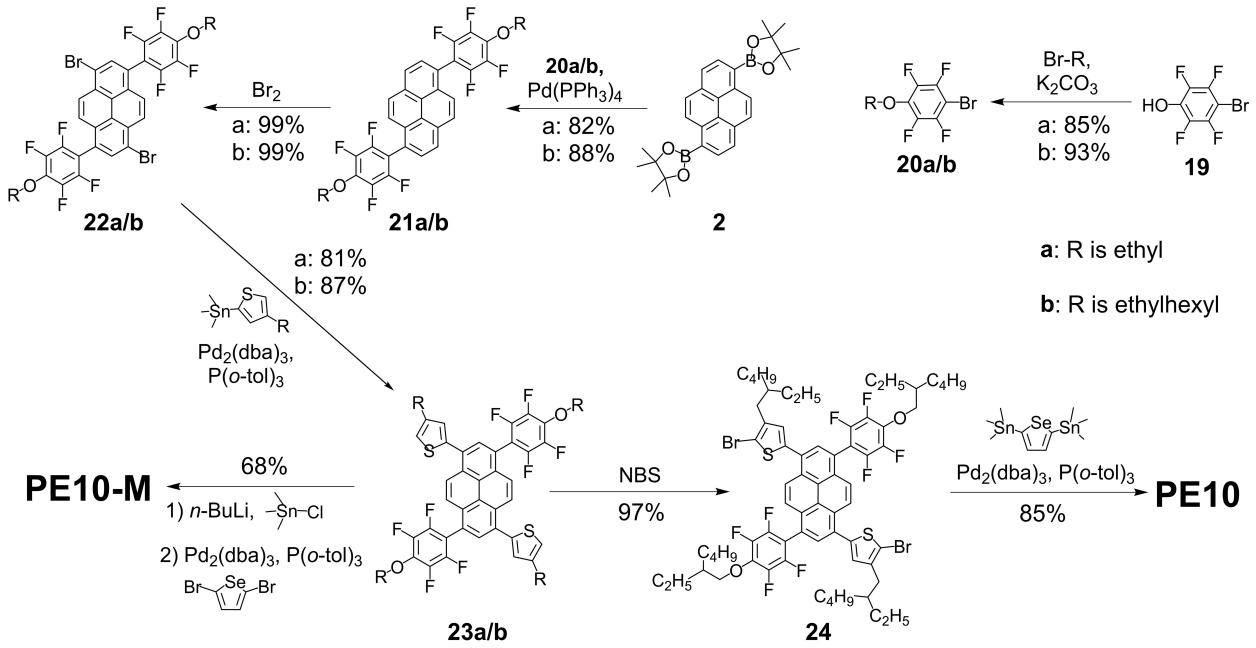

Scheme 1. Synthetic route to **PE** polymer and **PE-M** model molecules. Herein, **PE10** and **PE10-M** were illustrated for an example.

materials, indicating their great potential for low-cost and large-scale production. The average molecular weights (M_n) of **PE7**–**PE10** were estimated to be 34, 39, 39 and 38 kDa, along with the polydispersity indexes of 1.43, 1.20, 1.18 and 1.19, respectively. In view of the physiochemical property of polymers is greatly affected by molecular weights, the corresponding model molecules (Figure 2a, **PE7-M**–**PE10-M**) with well-defined structures were firstly synthesized to exclude the interferences from diverse molecular weights and make a clearer comparison. As displayed in Figure 2b and Figure S1, the relatively planar geometries can be indeed afforded by all the molecular backbones, but there is a large dihedral angle between pyrene and the side-attached benzene of 55° for **PE7-M** and **PE8-M**, and 63° for **PE9-M** and **PE10-M**. The planar backbone could enhance the intermolecular π–π stacking of polymers and the large dihedral angles with side phenyl groups here will be in favor of improving solubility significantly. When further enlarging the dihedral angle from thermodynamically stable states to 180 degrees in a simplified model (Figure 2c), a much larger energy barrier (ΔE) can be afforded by **PE9-M** and **PE10-M** in comparison to that of **PE7-M** and **PE8-M**. This suggests that fluorine substitution at pyrene-neighboring side can constrain the configuration variation caused by the single bond-connected phenyls greatly, which will be in favor of smaller reorganization energies and higher hole mobilities.[8c,11] The electrostatic surface potential maps (ESPs) of molecules unveil the decreased electron-rich property after fluorine substitutions due to the large electronegativity of fluorine, resulting in the stepwise downshifted highest occupied molecular orbitals (HOMOs) from **PE7-M** to **PE10-M** (Figure 2d). Note that a deep HOMO of HTM could contribute to a larger open-circuit voltage (V_{OC}) of PSCs in theory if sufficient driving force for hole extraction is guaranteed. As we know that the tight intermolecular packing of HTM is essential to achieve efficient charge transport and the degree of molecular aggregation can be roughly evaluated by investigating the temperature-dependent absorption spectra.[12] As illustrated in Figure 2e, **PE9-M** and **PE10-M** exhibit more bathochromically-shifted absorption peaks (by ≈12 nm) than that of **PE7-M** and **PE8-M** (by ≈8 nm) when cooling the corresponding solutions down to 10 degree from 100, suggesting stronger molecular aggregation of **PE9-M** and **PE10-M**. The similar tendency could be also observed in the UV/Vis spectra of corresponding polymers (Figure S2), thus expecting the possibly more efficient charge transport in HTM films.

From model molecules to their corresponding polymers, all the pyrene based polymers possess a good solubility in the commonly used processing solvent of chlorobenzene, satisfying the following solution-processing procedure for device fabrication. To monitor the phase and chemical stability of polymer films under thermal stress, we conducted the differential scanning calorimetry and thermal gravimetric analysis (Figure S3). No great phase transition was observed under 300 °C and the decomposition temperatures were estimated to be 423, 415, 416, 402 °C for **PE7**–**PE10**, respectively, indicating the excellent thermal stability but quite low crystallinity for all the four polymers. The derived HOMOs of polymer films from CVs (Figure S4a) are −5.25, −5.28, −5.32 and −5.34 eV for **PE7**–**PE10**, respectively, where the tendency is in accordance with the results derived from the ultraviolet photoelectron spectra (Figure S5). The HOMO energy levels of four polymers demonstrate adequate driving force for hole extractions with respect to that of −5.43 eV for perovskites as illustrated in Figure S4b. Figure S6 displayed highly similar absorption spectra of polymers in diluted chlorobenzene solutions, whereas much

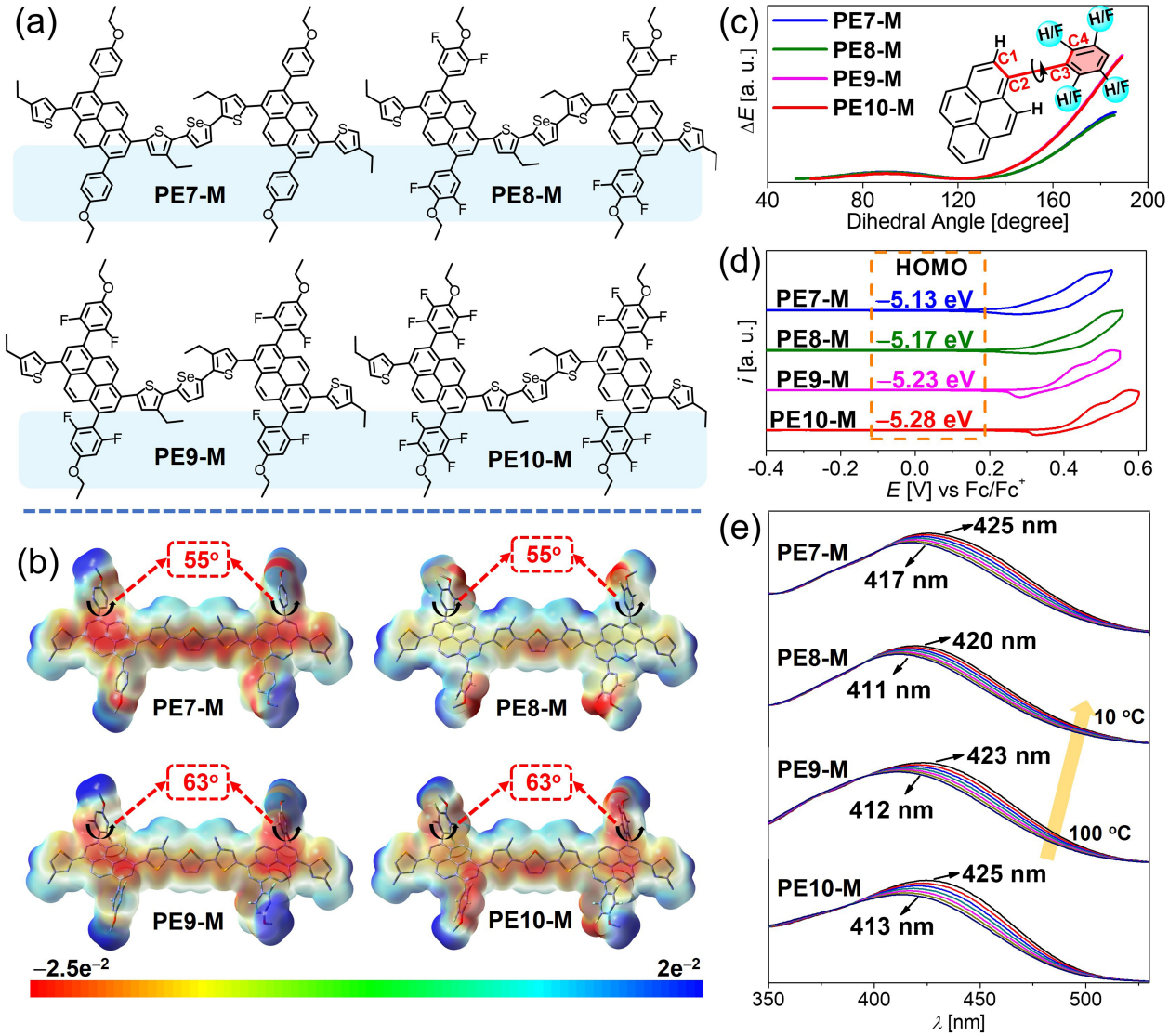

Figure 2. a) Model molecules synthesized for the pyrene polymers; b) optimized geometries and ESPs afforded by density functional theory (DFT) calculations. The dihedral angles between pyrene and benzene were highlighted; c) energy barriers (ΔE) of enlarging dihedral angle of C1-C2-C3-C4 from thermodynamically stable states to 180 degrees; d) cyclic voltammetry (CV) measured in solutions; e) variable-temperature absorption spectra in chlorobenzene.

different ones in solid states, suggesting the diverse molecular stacking models in polymer films.[8a] Therefore, grazing-incidence wide-angle X-ray scattering (GIWAXS) measurement was performed to shed light on the different molecular stacking induced by fluorine substitution (Figure S7). As shown in Figure 3a, **PE7** and **PE8** prefer to stack with a typical edge-on orientation as indicated by the strong peaks at $q_z \approx 0.29$ Å^{-1},[13] but it is worth noting that a stacking model transition from edge-on to more favorable face-on orientations can be observed in **PE9** and **PE10** films. In view of the same polymeric backbones, this preferred face-on molecular stacking of **PE9** and **PE10** should be attributed to the better intersecting distribution of pyrene and benzene planes, which places the fluorine atoms directly above pyrene plane through a possible strong intermolecular fluorine–aromatic (F–π) actions.[10] In addition, a smaller π–π stacking distance of ≈4.3 Å can be observed by **PE8**–**PE10** with respect to that of 4.5 Å for **PE7** without the fluorine substitution. All the above advantages contribute to the stepwise enlarged hole mobilities of 7.64×10^{-4}, 1.02×10^{-3}, 1.21×10^{-3} and 1.46×10^{-3} cm^{2}V^{-1}s^{-1} for **PE7**–**PE10**, respectively (Figure S8), which can be expected to achieve improved charge transport in HTM layer and optimized fill factors (FFs) in resulting PSCs.[14] The detailed parameters of optical, thermal and electrochemical properties for polymers were listed in Table S1.

To visualize film morphologies of polymeric HTM layers when coated on a perovskite film, the atomic force microscopy was carried out, demonstrating the much smaller root-mean-square roughness of 10–12 nm for polymer-coated perovskite films comparing to that of ≈20 nm for neat perovskite one (Figure S9). The uniform coverage by hydro-

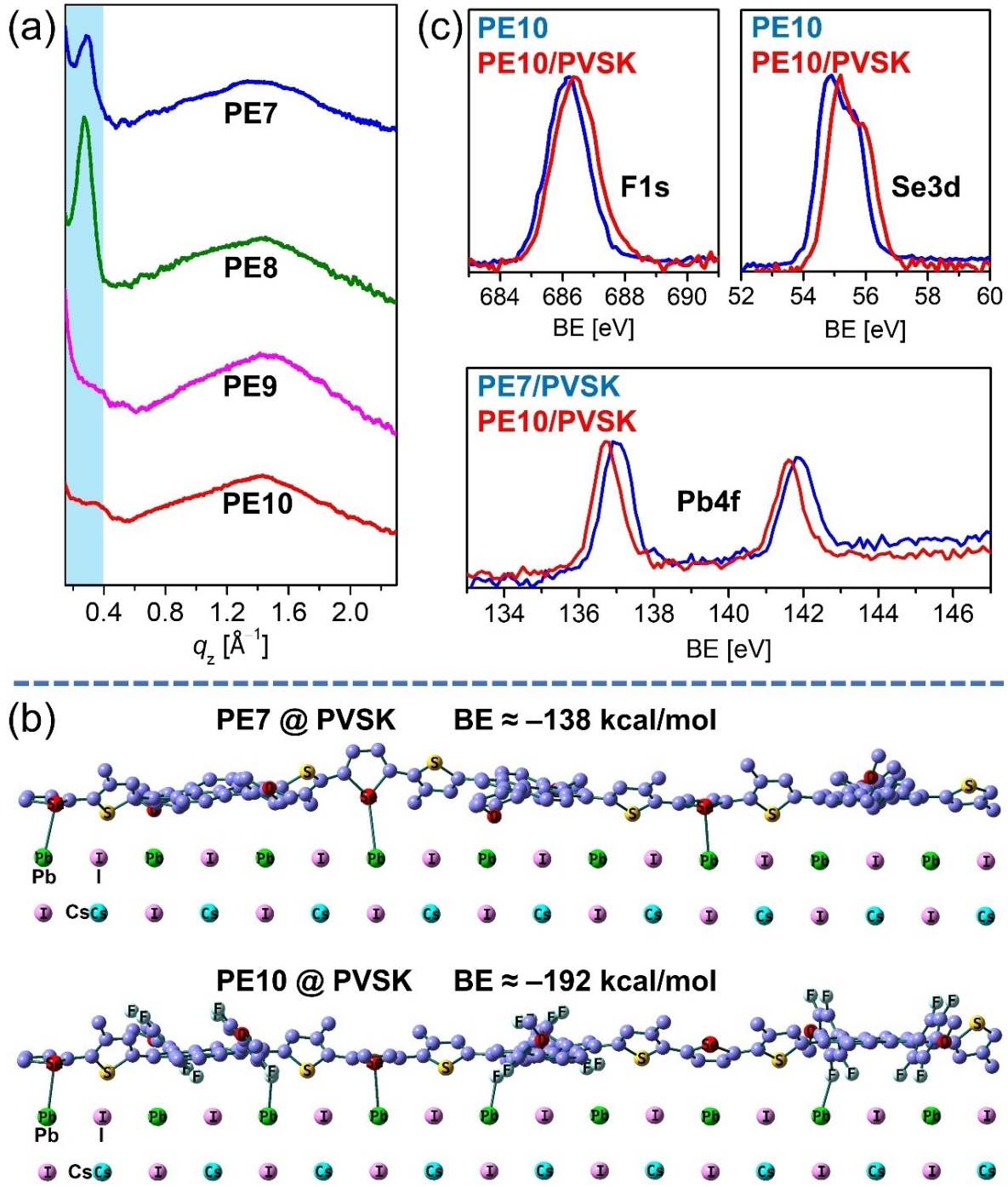

Figure 3. a) Out-of-plane line cuts of 2D GIWAXS for polymers on silicon substrates; b) theoretically modeled stacking patterns of polymers on top of a perovskite (PVSK) surface. The color balls of green: Pb; magenta: I; cyan: Cs; c) XPS signals of F 1s and Se 3d from a pristine **PE10** film and a **PE10** coated perovskite film and also XPS signals of Pb 4f from **PE7**- and **PE10**-coated perovskite films.

phobic polymers could protect perovskite from direct contact with moisture in the surrounding environment, promoting the long-term stability of PSCs.[8] As we know that the efficient interfacial charge transfer through the tight contact between HTMs and perovskite is necessary in the state-of-the-art PSCs. That is why 2D pyrene and easy polarizable selenium[8b] were selected as the main building blocks here as we have discussed above. DFT calculations in Figure 3b and S10 show that **PE** polymers could pack with perovskite surface compact trough the broad 2D conjugated plane of pyrene. Moreover, the selenium and fluorine atoms in **PE10** are prone to approach lead sites on perovskite surface to have a weak but specific secondary interaction. The combined two factors above result in much enlarged binding energy of $-192\,\mathrm{kcal\,mol^{-1}}$ for **PE10**@PVSK in comparison to that of $-138\,\mathrm{kcal\,mol^{-1}}$ for **PE7**@PVSK

without fluorine substitution. This tight packing between HTMs and perovskite surface could render an sufficient orbital overlaps at perovskite/HTM interface and thus passivate the coordinatively unsaturated lead ion efficiently.[15] The efficient interfacial passivation can be further indicated by the obvious shifting of characteristic peaks of X-ray photoelectron spectroscopy (XPS) for F 1s, Se 3d and Pb 4f orbitals (Figure 3c).[8b,16] Note that the sufficient interfacial passivation is expected to decrease the recombination centers at perovskite/HTM interface and thus afford a better PSC.[17] Therefore, we further measured the trap state densities of **PE** polymer-coated perovskite films (Figure S11) and estimated the trap state density to be 1.20×10^{-16}, 0.48×10^{-16}, 0.28×10^{-16}, 0.21×10^{-16}, 0.17×10^{-16} cm^{-3}, respectively for pristine, **PE7**-coated, **PE8**-coated, **PE9**-coated and **PE10**-coated perovskite films. The significantly decreased trap state densities of perovskite films coated by the polymeric HTMs demonstrate the sufficient interfacial passivation. Moreover, from **PE7** to **PE10**, the trap state densities reduced from 0.48×10^{-16} to 0.17×10^{-16} cm^{-3}, which should be attributed to the different position and number of fluorine atoms on the same polymeric backbone. The tendency of trap state density variation agrees well with the results of XPS and DFT simulations discussed above.

As shown in Figure 4a, due to the well-matched energy levels, tight interfacial contacts and sufficient passivation at the energy-offset HTM/perovskite interface, the extensive PL quenching of perovskite films when capped with polymeric HTMs can be observed, indicating the highly efficient hole extraction. This is in good accordance with the significantly reduced lifetime of **PE** polymers coated perovskite film comparing to that of the pristine one, which can be obviously noted from their time resolved photoluminescence decay curves (Figure S12 and Table S2). Then PSCs with a regular architecture of glass/FTO/SnO_2/perovskite ($MAPbI_3$)/HTM/Au were fabricated to evaluate the potential of **PE** polymers as dopant-free HTMs. Figure 4b recorded *J–V* curves of PSCs based on dopant-free polymers (see Table 1 for detailed parameters). From **PE7** to **PE10**, stepwise enlarged V_{OC} and FFs can be afforded, contributing to the PCEs of 18.5 % for **PE7**, 19.0 % for **PE8**, 19.8 % for **PE9** and 21.0 % for **PE10**. The amplification of V_{OC} agrees well with the downshifted HOMOs and enhanced interfacial passivation from **PE7** to **PE10**, while the improved FFs should be attributed to the escalating hole mobilities. Note that very similar short-circuit current densities (J_{SC}) of ≈23 mA cm^{-2} can be observed and are in good agreement with the integrated current densities from spectra of external quantum efficiencies (EQEs) in Figure 4c. To further elucidate the origin of V_{OC} and FF enlargements, we carried out the electrochemical impedance spectroscopy (Figure S13). The charge transport resistance (R_H) at a given bias voltage shows the tendency of **PE10** < **PE9** < **PE8** < **PE7**, however, the recombination resistance (R_{rec}) displays the opposite arrangement of **PE10** > **PE9** > **PE8** > **PE7**. The lower R_H and higher R_{rec} of **PE10** based device will certainly facilitate the charge transport and depress the charge recombination, accounting for its improved PCE.[18] It is also worth mentioning that the best performance of PSCs was achieved with a low HTM concentration of ≈5 mg mL^{-1}, much less than that of 60–80 mg mL^{-1} for typical spiro-OMeTAD.[1g] Meanwhile, the statistical analysis for three batches of **PE10** demonstrates an excellent synthetic and device reproducibility (Figure S14). The low consumption/cost and good reproducibility of HTMs should possess the great importance no less than high PCEs of PSCs, when taking the ultimate aim of commercial application into consideration.

In light of the great potential as highly efficient dopant-free HTM for **PE10**, we further evaluated its performance in PSCs with an architecture of glass/ITO/SnO_2/perovskite ($FA_{0.85}MA_{0.15}PbI_3$)/HTM/MoO_3/Ag. Owing to the broader absorption and longer carrier lifetimes of mixed perovskite,[19] the resulting PSCs give rise to a fully upgraded J_{SC} of 24.1 mA cm^{-2}, V_{OC} of 1.16 V and FF of 79.8 %, leading to an impressive PCE of 22.3 % with highly stable output of J_{SC} and PCE (Figure 4d–f), along with little hysteresis simultaneously (Figure S15). This has ranked **PE10** based PSCs among the best PSCs based on dopant-free HTMs. The *J–V* curves and photovoltaic parameters of PSCs based on mixed perovskite and **PE7**–**PE9** were displayed in Figure S16. Much a larger contact angle ($\approx100°$) could be recorded when putting a water droplet on **PE** polymer-capped perovskite films with respect to that of $\approx60°$ on neat perovskite, suggesting enough protection of hygroscopic perovskite from moisture in surrounding environment (Figure S17). Therefore, the un-encapsulated PSCs capped with **PE10** were firstly placed at 40 °C under continuous illumination for 1000 h. As displayed in Figure 4g, in sharp contrast to the dramatic decrease of control PSCs coated by doped Spiro-OMeTAD, the PSCs utilizing dopant-free **PE10** as HTM maintained a good PCE over 90 %. In order to further evaluate the thermal stability, PSCs have been stored at

Table 1: Photovoltaic parameters of PSCs based on dopant-free **PE** series HTMs under the illumination of AM 1.5G (100 mW cm^{-2}).[a]

HTMs	$J_{SC\text{-}EQE}$ [mA cm^{-2}]	J_{SC} [mA cm^{-2}]	V_{OC} [V]	*FF* [%]	*PCE* [%]
PE7	22.2 ± 0.2	22.8 ± 0.3	1.07 ± 0.02	76.0 ± 0.8	18.3 ± 0.2 (18.5)
PE8	22.6 ± 0.3	22.7 ± 0.2	1.09 ± 0.01	76.6 ± 1.4	18.7 ± 0.3 (19.0)
PE9	22.7 ± 0.2	23.0 ± 0.1	1.11 ± 0.01	77.6 ± 1.1	19.6 ± 0.2 (19.8)
PE10	23.0 ± 0.2	23.2 ± 0.3	1.13 ± 0.02	80.1 ± 0.6	20.9 ± 0.1 (21.0)
PE10	23.7 ± 0.3	24.1 ± 0.2	1.16 ± 0.02	79.8 ± 0.6	22.1 ± 0.2 (22.3)[b]

[a] $J_{SC\text{-}EQE}$ was calculated via wavelength integration of the standard AM1.5G emission spectrum. The best PCEs were included in the brackets.
[b] The parameters based on a mixed perovskite of $FA_{0.85}MA_{0.15}PbI_3$.

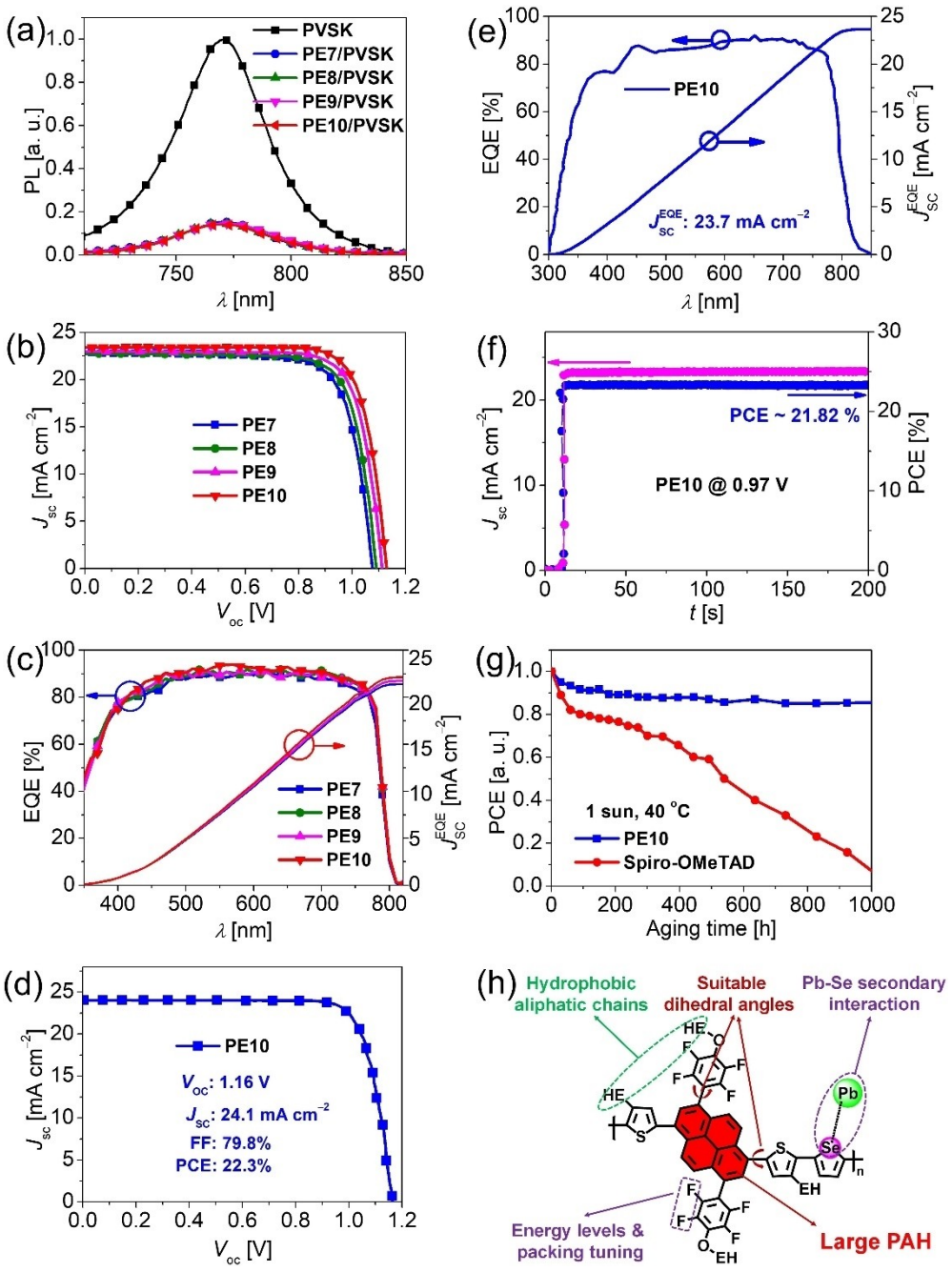

Figure 4. a) Steady-state PL spectra of PVSK and HTM-capped PVSK; b), d) *J–V* curves and c), e) EQEs curves for PSCs with pure and mixed perovskite, respectively; f) steady-state output of J_{SC} and PCE at MPP under continuous illumination of AM 1.5G; g) PCE variation of PSCs employing doped Spiro-OMeTAD and dopant-free **PE10** irradiated continuously under one sunlight at 40 °C and 30–60% relative humidity; h) structure–function relation analysis of **PE10**.

85 °C with or without sunlight irradiation. As illustrated in Figure S18 and Table S3, limited by the intrinsic instability of perovskite crystal, an obvious PCE drop after 200 h can be observed. However, the PSCs with dopant-free **PE10** as the HTM still exhibited a much better PCE retention with respect to that of control PSCs with doped Spiro-OMeTAD. In addition, the cost analysis for preparation of **PE10** were carried out and presented in Scheme S5–S8 and Table S4, S5. Note that several key intermediates for **PE10** synthesis are not commercially available at the current stage, which inevitably force the preparation costs up, whereas, the great material assuming advantage for per cell ($\approx$5 mg mL^{-1} for **PE10** without any dopants, 60–80 mg mL^{-1} for Spiro-OMeTAD with lithium salts and cobalt complexes as dopants) still renders **PE10** highly promising for large-scale production of PSCs. To sum up, in a well-designed dopant-free polymeric HTM like **PE10** or others, we believe that several key structural elements should be addressed (Figure 4h):

1) 2D PAHs to enhance the intermolecular π–π stacking and also packing with perovskite surface; 2) a delicate balance between enough hydrophobic aliphatic chains to improve humidity resistivity of PSCs and molecular packing; 3) "Lewis soft" atoms, e.g. Se, to passivate trap state states on perovskite surface; 4) suitable dihedral angles to guarantee the adequate solubility on condition that high hole mobility can be achieved; 5) fluorine atoms to tune energy levels and molecular packing.

Conclusion

To address the adverse effects of dopants in HTM layer on device performance of PSCs, a new class of distinctive dopant-free polymeric HTMs were developed by incorporating 2D pyrene into thiophene and selenophene repeat conjugated chains. With the aid of broad plane of pyrene and specific Pb–Se secondary interaction, not only the efficient charge transport in HTM layer, but also improved charge transfer and passivation at perovskite/HTM interface could be reached. More interestingly, fluorine substitution at pyrene-neighboring position can boost the molecular stacking of HTMs towards a more favorable face-on orientation, unveiling its non-negligible role in morphology control of HTMs. Consequently, PSCs utilizing **PE10** as a dopant-free HTM afford an excellent PCE of 22.3 % accompanied with markedly improved device durability under dual pressure of thermal and irradiation, ranking it among the best PSCs based on dopant-free HTMs. Our work has afforded an excellent dopant-free HTM platform for PSCs and will stimulate further innovative explorations for polymeric HTMs with both high efficiency and low-cost, aiming to boost PSCs towards commercial application.

Supporting Information

Detailed description of the experimental methods, including molecular synthesis, film deposition, device fabrication and characterization, additional data and figures, and NMR spectra. This material is available free of charge via the Internet.

Acknowledgements

This work was financially supported by the 100 Young Academic Leaders Program of Nankai University (Grants No. 020-63213096), the Swedish Energy Agency, MoST (2019YFA0705900), NSFC of China (21935007) and Zhejiang Province Selected Funding for Postdoctoral Research Projects (ZJ2021001). We also acknowledge the National Supercomputer Centre at Linköping University and Westlake University HPC center for computation resources and also the Instrumentation and Service Center for Physical Sciences at Westlake University for facility support and technical assistance.

Conflict of Interest

The authors declare no competing financial interest.

Data Availability Statement

The data that support the findings of this study are available from the corresponding author upon reasonable request.

Keywords: Dopant-Free Pyrene Polymers · Fluorine-Substituted Polymers · Interfacial Passivation · Molecular Stacking Control · Perovskite Solar Cells

[1] a) A. Kojima, K. Teshima, Y. Shirai, T. Miyasaka, *J. Am. Chem. Soc.* **2009**, *131*, 6050–6051; b) H.-S. Kim, C.-R. Lee, J.-H. Im, K.-B. Lee, T. Moehl, A. Marchioro, S.-J. Moon, R. Humphry-Baker, J.-H. Yum, J. E. Moser, M. Grätzel, N.-G. Park, *Sci. Rep.* **2012**, *2*, 591; c) W. S. Yang, B.-W. Park, E. H. Jung, N. J. Jeon, Y. C. Kim, D. U. Lee, S. S. Shin, J. Seo, E. K. Kim, J. H. Noh, S. I. Seok, *Science* **2017**, *356*, 1376–1379; d) Q. Jiang, Y. Zhao, X. Zhang, X. Yang, Y. Chen, Z. Chu, Q. Ye, X. Li, Z. Yin, J. You, *Nat. Photonics* **2019**, *13*, 460–466; e) A. K. Jena, A. Kulkarni, T. Miyasaka, *Chem. Rev.* **2019**, *119*, 3036–3103; f) M. Jeong, I. W. Choi, E. M. Go, Y. Cho, M. Kim, B. Lee, S. Jeong, Y. Jo, H. W. Choi, J. Lee, J.-H. Bae, S. K. Kwak, D. S. Kim, C. Yang, *Science* **2020**, *369*, 1615–1620; g) N. Li, X. Niu, L. Li, H. Wang, Z. Huang, Y. Zhang, Y. Chen, X. Zhang, C. Zhu, H. Zai, Y. Bai, S. Ma, H. Liu, X. Liu, Z. Guo, G. Liu, R. Fan, H. Chen, J. Wang, Y. Lun, X. Wang, J. Hong, H. Xie, D. S. Jakob, X. G. Xu, Q. Chen, H. Zhou, *Science* **2021**, *373*, 561–567; h) Y. Zhong, G. Liu, Y. Su, W. Sheng, L. Gong, J. Zhang, L. Tan, Y. Chen, *Angew. Chem. Int. Ed.* **2022**, *61*, e202114588; *Angew. Chem.* **2022**, *134*, e202114588; i) R. Lin, J. Xu, M. Wei, Y. Wang, Z. Qin, Z. Liu, J. Wu, K. Xiao, B. Chen, S. M. Park, G. Chen, H. R. Atapattu, K. R. Graham, J. Xu, J. Zhu, L. Li, C. Zhang, E. H. Sargent, H. Tan, *Nature* **2022**, *603*, 73–78.

[2] a) J. H. Noh, N. J. Jeon, Y. C. Choi, M. K. Nazeeruddin, M. Grätzel, S. I. Seok, *J. Mater. Chem. A* **2013**, *1*, 11842–11847; b) A. Abate, T. Leijtens, S. Pathak, J. Teuscher, R. Avolio, M. E. Errico, J. Kirkpatrik, J. M. Ball, P. Docampo, I. McPherson, H. J. Snaith, *Phys. Chem. Chem. Phys.* **2013**, *15*, 2572–2579; c) J. Burschka, A. Dualeh, F. Kessler, E. Baranoff, N.-L. Cevey-Ha, C. Yi, M. K. Nazeeruddin, M. Grätzel, *J. Am. Chem. Soc.* **2011**, *133*, 18042–18045; d) T. Leijtens, J. Lim, J. Teuscher, T. Park, H. J. Snaith, *Adv. Mater.* **2013**, *25*, 3227–3233.

[3] a) F. Fabregat-Santiago, J. Bisquert, L. Cevey, P. Chen, M. Wang, S. M. Zakeeruddin, M. Grätzel, *J. Am. Chem. Soc.* **2009**, *131*, 558–562; b) J. Liu, Y. Wu, C. Qin, X. Yang, T. Yasuda, A. Islam, K. Zhang, W. Peng, W. Chen, L. Han, *Energy Environ. Sci.* **2014**, *7*, 2963–2967.

[4] a) A. K. Jena, M. Ikegami, T. Miyasaka, *ACS Energy Lett.* **2017**, *2*, 1760–1761; b) G. Parthasarathy, C. Shen, A. Kahn, S. R. Forrest, *J. Appl. Phys.* **2001**, *89*, 4986–4992; c) E. J. Juarez-Perez, M. R. Leyden, S. Wang, L. K. Ono, Z. Hawash, Y. Qi, *Chem. Mater.* **2016**, *28*, 5702–5709.

[5] a) K. Rakstys, S. Paek, P. Gao, P. Gratia, T. Marszalek, G. Grancini, K. T. Cho, K. Genevicius, V. Jankauskas, W. Pisula, M. K. Nazeeruddin, *J. Mater. Chem. A* **2017**, *5*, 7811–7815; b) B. Xu, D. Bi, Y. Hua, P. Liu, M. Cheng, M. Grätzel, L. Kloo, A. Hagfeldt, L. Sun, *Energy Environ. Sci.* **2016**, *9*, 873–877; c) C. Huang, W. Fu, C.-Z. Li, Z. Zhang, W. Qiu, M. Shi, P.

Heremans, A. K. Y. Jen, H. Chen, *J. Am. Chem. Soc.* **2016**, *138*, 2528–2531; d) W. Zhou, Z. Wen, P. Gao, *Adv. Energy Mater.* **2018**, *8*, 1702512; e) N. Cai, F. Li, Y. Chen, R. Luo, T. Hu, F. Lin, S.-M. Yiu, D. Liu, D. Lei, Z. Zhu, A. K.-Y. Jen, *Angew. Chem. Int. Ed.* **2021**, *60*, 20437–20442; *Angew. Chem.* **2021**, *133*, 20600–20605; f) H. Guo, H. Zhang, C. Shen, D. Zhang, S. Liu, Y. Wu, W.-H. Zhu, *Angew. Chem. Int. Ed.* **2021**, *60*, 2674–2679; *Angew. Chem.* **2021**, *133*, 2706–2711; g) V. A. Chiykowski, Y. Cao, H. Tan, D. P. Tabor, E. H. Sargent, A. Aspuru-Guzik, C. P. Berlinguette, *Angew. Chem. Int. Ed.* **2018**, *57*, 15529–15533; *Angew. Chem.* **2018**, *130*, 15755–15759; h) E. H. Jung, N. J. Jeon, E. Y. Park, C. S. Moon, T. J. Shin, T.-Y. Yang, J. H. Noh, J. Seo, *Nature* **2019**, *567*, 511–515; i) F. Liu, F. Wu, Z. Tu, Q. Liao, Y. Gong, L. Zhu, Q. Li, Z. Li, *Adv. Funct. Mater.* **2019**, *29*, 1901296; j) H. Lu, B. He, Y. Ji, Y. Shan, C. Zhong, J. Xu, J. LiuYang, F. Wu, L. Zhu, *Chem. Eng. J.* **2020**, *385*, 123976; k) Y. Li, F. Wu, M. Han, Z. Li, L. Zhu, Z. Li, *ACS Energy Lett.* **2021**, *6*, 869–876.

[6] a) W. Hou, Y. Xiao, G. Han, J.-Y. Lin, *Polymer* **2019**, *11*, 143; b) M. Al-Hussein, E. M. Herzig, M. Schindler, F. Löhrer, C. M. Palumbiny, W. Wang, S. V. Roth, P. Müller-Buschbaum, *Polym. Eng. Sci.* **2016**, *56*, 889–894; c) B. Su, H. A. Caller-Guzman, V. Körstgens, Y. Rui, Y. Yao, N. Saxena, G. Santoro, S. V. Roth, P. Müller-Buschbaum, *ACS Appl. Mater. Interfaces* **2017**, *9*, 43724–43732; d) X. Sun, X. Yu, Z. a. Li, *ACS Appl. Energy Mater.* **2020**, *3*, 10282–10302; e) Q. Fu, Z. Xu, X. Tang, T. Liu, X. Dong, X. Zhang, N. Zheng, Z. Xie, Y. Liu, *ACS Energy Lett.* **2021**, *6*, 1521–1532.

[7] a) G. You, Q. Zhuang, L. Wang, X. Lin, D. Zou, Z. Lin, H. Zhen, W. Zhuang, Q. Ling, *Adv. Energy Mater.* **2020**, *10*, 1903146; b) F. Qi, X. Deng, X. Wu, L. Huo, Y. Xiao, X. Lu, Z. Zhu, A. K.-Y. Jen, *Adv. Energy Mater.* **2019**, *9*, 1902600; c) J. Lee, G.-W. Kim, M. Kim, S. A. Park, T. Park, *Adv. Energy Mater.* **2020**, *10*, 1902662; d) M. J. Jeong, K. M. Yeom, S. J. Kim, E. H. Jung, J. H. Noh, *Energy Environ. Sci.* **2021**, *14*, 2419–2428; e) Y. Zhang, Y. Ren, X. Xie, Y. Wei, L. He, L. Fang, J. Zhang, Y. Yuan, P. Wang, *Adv. Funct. Mater.* **2021**, *31*, 2108855; f) H.-C. Liao, T. L. D. Tam, P. Guo, Y. Wu, E. F. Manley, W. Huang, N. Zhou, C. M. M. Soe, B. Wang, M. R. Wasielewski, L. X. Chen, M. G. Kanatzidis, A. Facchetti, R. P. H. Chang, T. J. Marks, *Adv. Energy Mater.* **2016**, *6*, 1600502; g) L. Zhang, C. Liu, J. Zhang, X. Li, C. Cheng, Y. Tian, A. K.-Y. Jen, B. Xu, *Adv. Mater.* **2018**, *30*, 1804028; h) F. Cai, J. Cai, L. Yang, W. Li, R. S. Gurney, H. Yi, A. Iraqi, D. Liu, T. Wang, *Nano Energy* **2018**, *45*, 28–36; i) K. Kranthiraja, K. Gunasekar, H. Kim, A.-N. Cho, N.-G. Park, S. Kim, B. J. Kim, R. Nishikubo, A. Saeki, M. Song, S.-H. Jin, *Adv. Mater.* **2017**, *29*, 1700183.

[8] a) F. Zhang, Z. Yao, Y. Guo, Y. Li, J. Bergstrand, C. J. Brett, B. Cai, A. Hajian, Y. Guo, X. Yang, J. M. Gardner, J. Widengren, S. V. Roth, L. Kloo, L. Sun, *J. Am. Chem. Soc.* **2019**, *141*, 19700–19707; b) Z. Yao, F. Zhang, Y. Guo, H. Wu, L. He, Z. Liu, B. Cai, Y. Guo, C. J. Brett, Y. Li, C. V. Srambickal, X. Yang, G. Chen, J. Widengren, D. Liu, J. M. Gardner, L. Kloo, L. Sun, *J. Am. Chem. Soc.* **2020**, *142*, 17681–17692; c) Y. Guo, L. He, J. Guo, Y. Guo, F. Zhang, L. Wang, H. Yang, C. Xiao, Y. Liu, Y. Chen, Z. Yao, L. Sun, *Angew. Chem. Int. Ed.* **2022**, *61*, e202114341; *Angew. Chem.* **2022**, *134*, e202114341.

[9] a) T. M. Figueira-Duarte, K. Müllen, *Chem. Rev.* **2011**, *111*, 7260–7314; b) N. J. Jeon, J. Lee, J. H. Noh, M. K. Nazeeruddin, M. Grätzel, S. I. Seok, *J. Am. Chem. Soc.* **2013**, *135*, 19087–19090.

[10] a) S.-i. Kawahara, S. Tsuzuki, T. Uchimaru, *J. Phys. Chem. A* **2004**, *108*, 6744–6749; b) P. Li, J. M. Maier, E. C. Vik, C. J. Yehl, B. E. Dial, A. E. Rickher, M. D. Smith, P. J. Pellechia, K. D. Shimizu, *Angew. Chem. Int. Ed.* **2017**, *56*, 7209–7212; *Angew. Chem.* **2017**, *129*, 7315–7318.

[11] R. A. Marcus, *Angew. Chem. Int. Ed. Engl.* **1993**, *32*, 1111–1121; *Angew. Chem.* **1993**, *105*, 1161–1172.

[12] F. Panzer, H. Bässler, A. Köhler, *J. Phys. Chem. Lett.* **2017**, *8*, 114–125.

[13] P. Müller-Buschbaum, *Adv. Mater.* **2014**, *26*, 7692–7709.

[14] Z. Wang, K. Gao, Y. Kan, M. Zhang, C. Qiu, L. Zhu, Z. Zhao, X. Peng, W. Feng, Z. Qian, X. Gu, A. K. Y. Jen, B. Z. Tang, Y. Cao, Y. Zhang, F. Liu, *Nat. Commun.* **2021**, *12*, 332.

[15] a) J. Luo, J. Xia, H. Yang, L. Chen, Z. Wan, F. Han, H. A. Malik, X. Zhu, C. Jia, *Energy Environ. Sci.* **2018**, *11*, 2035–2045; b) B. X. Zhao, C. Yao, K. Gu, T. Liu, Y. Xia, Y.-L. Loo, *Energy Environ. Sci.* **2020**, *13*, 4334–4343.

[16] a) R. Wang, J. Xue, K.-L. Wang, Z.-K. Wang, Y. Luo, D. Fenning, G. Xu, S. Nuryyeva, T. Huang, Y. Zhao, J. L. Yang, J. Zhu, M. Wang, S. Tan, I. Yavuz, K. N. Houk, Y. Yang, *Science* **2019**, *366*, 1509–1513; b) L. Fang, A. Zheng, M. Ren, X. Xie, P. Wang, *ACS Appl. Mater. Interfaces* **2019**, *11*, 39001–39009.

[17] a) J. Peng, Y. Wu, W. Ye, D. A. Jacobs, H. Shen, X. Fu, Y. Wan, T. Duong, N. Wu, C. Barugkin, H. T. Nguyen, D. Zhong, J. Li, T. Lu, Y. Liu, M. N. Lockrey, K. J. Weber, K. R. Catchpole, T. P. White, *Energy Environ. Sci.* **2017**, *10*, 1792–1800; b) F. Li, X. Deng, F. Qi, Z. Li, D. Liu, D. Shen, M. Qin, S. Wu, F. Lin, S.-H. Jang, J. Zhang, X. Lu, D. Lei, C.-S. Lee, Z. Zhu, A. K. Y. Jen, *J. Am. Chem. Soc.* **2020**, *142*, 20134–20142; c) S. Gharibzadeh, P. Fassl, I. M. Hossain, P. Rohrbeck, M. Frericks, M. Schmidt, T. Duong, M. R. Khan, T. Abzieher, B. A. Nejand, F. Schackmar, O. Almora, T. Feeney, R. Singh, D. Fuchs, U. Lemmer, J. P. Hofmann, S. A. L. Weber, U. W. Paetzold, *Energy Environ. Sci.* **2021**, *14*, 5875–5893; d) B. Yang, J. Suo, F. Di Giacomo, S. Olthof, D. Bogachuk, Y. Kim, X. Sun, L. Wagner, F. Fu, S. M. Zakeeruddin, A. Hinsch, M. Grätzel, A. Di Carlo, A. Hagfeldt, *ACS Energy Lett.* **2021**, *6*, 3916–3923; e) E. Li, C. Liu, H. Lin, X. Xu, S. Liu, S. Zhang, M. Yu, X.-M. Cao, Y. Wu, W.-H. Zhu, *Adv. Funct. Mater.* **2021**, *31*, 2103847; f) X. Xu, X. Ji, R. Chen, F. Ye, S. Liu, S. Zhang, W. Chen, Y. Wu, W.-H. Zhu, *Adv. Funct. Mater.* **2022**, *32*, 2109968.

[18] V. Gonzalez-Pedro, E. J. Juarez-Perez, W.-S. Arsyad, E. M. Barea, F. Fabregat-Santiago, I. Mora-Sero, J. Bisquert, *Nano Lett.* **2014**, *14*, 888–893.

[19] H. F. Zarick, N. Soetan, W. R. Erwin, R. Bardhan, *J. Mater. Chem. A* **2018**, *6*, 5507–5537.

Manuscript received: February 3, 2022
Accepted manuscript online: March 19, 2022
Version of record online: April 12, 2022